MOLECULAR AND CELLULAR BIOLOGY, Oct. 2008, p. 6439–6451 Vol. 28, No. 20
0270-7306/08/$08.00+0 doi:10.1128/MCB.00727-08
Copyright © 2008, American Society for Microbiology. All Rights Reserved.

An Allelic Series Uncovers Novel Roles of the BRCT Domain-Containing Protein PTIP in Mouse Embryonic Vascular Development[▽]

Weipeng Mu, Wei Wang, and John C. Schimenti*

Department of Biomedical Sciences, Cornell College of Veterinary Medicine, Ithaca, New York 14853

Received 7 May 2008/Returned for modification 11 June 2008/Accepted 9 August 2008

Pax transactivation domain-interacting protein (PTIP, or PAXIP1) is required for mouse development and has been implicated in DNA damage responses and histone modification. However, the physiological roles of PTIP during embryogenesis remain unclear due to early embryonic lethality of null mutants. We describe two *N*-ethyl *N*-nitrosourea-induced hypomorphic missense alleles of *Ptip*, each of which alters one of the six encoded BRCT domains. Phenotypic characterization of these mutants revealed important functions of PTIP in vasculogenesis and chorioplacental development that appear unrelated to activities in DNA repair or global histone modification. The results of gene expression profiling and in vitro angiogenesis assays indicated that PTIP modulates a transcriptional program, centered around *Vegfa*, that drives the migration of endothelial cells to properly form the embryonic vasculature. These and other data suggest that PTIP has multiple functions, one of which is to promote the formation of transcriptional complexes that provide specificity of developmental gene expression.

The formation of a normally patterned, functional vascular system is essential for embryogenesis. The development and physiological maturation of most organs is critically dependent on the accurate establishment of the vascular system (49). Two key sequential morphogenic processes underlie vascular development: (i) vasculogenesis, defined by the formation of primary capillary plexus from endothelial cells, and (ii) angiogenesis, characterized by neovascularization from preexisting vessels, such as the primary capillary plexus (48). Vascular formation is a dynamic and complicated process, and our understanding of the underlying mechanisms is incomplete.

Over the past 15 years, the functions of many genes involved in angiogenesis or vasculogenesis have been investigated by the application of gene targeting in mice. Most of these genes are components of signaling pathway networks, including *Vegf* (3, 11), *Ang*/*Tie* (10), *TGF*β/*Smad* (16), *Notch* (12, 25, 26), *integrin* (52), and *EphB*/*Ephrin* (1, 61), which temporally and spatially regulate the initiation, progression, and remodeling of vasculature. Gene targeting is not ideal for the unbiased discovery of new genes essential for this process. Forward genetic mutagenesis screens provide an alternative to the discovery of new genes causing cardiovascular phenotypes in both mice (67) and zebrafish (57) and can yield hypomorphic alleles that uncover developmental functions that are otherwise masked by early embryonic lethality caused by null alleles.

PTIP contains six BRCT domains and is essential for mitotic progression and embryonic development in mice (5, 30). BRCT domains are most often found in proteins involved in DNA repair. Null mutations of these genes, such as *Brca1* (51), *Bard1* (37), *Xrcc1* (58), and *Lig3* (47), often lead to embryonic lethality that is partially due to failure to repair DNA damage. Cells deficient in PTIP have increased sensitivity to DNA damage induced by ionizing radiation (24) and an attenuated response to replication stress-induced DNA damage (15). The C-terminal BRCT domains appear to be responsible for phosphorylation-dependent protein localization into 53BP1- and γH2AX-containing nuclear foci following the induction of DNA breaks (34). However, it is unknown whether the embryonic lethality of PTIP null mutants is directly attributable to defective DNA damage repair. The roles of the N-terminal BRCT domains are unknown.

While the functions of many BRCT domain-containing proteins in DNA damage response have been well studied, little is known about the physiological roles of PTIP during mammalian embryogenesis. The *Xenopus laevis* ortholog, SWIFT, has ~80% amino acid sequence identity with the BRCT domains of mouse PTIP. The inhibition of SWIFT results in the suppression of TGFβ-induced gene transcription and defective mesoderm formation (54). The results of recent studies showed that PTIP is a component of the histone H3K4 methyltransferase complex (22, 44). Histone H3 methylation levels were reported to be reduced in *Ptip* null mouse embryos (44), indicating the involvement of PTIP in the epigenetic regulation of embryogenesis. PTIP physically interacts with the Pax proteins, a group of DNA binding transcription factors that play crucial roles during organogenesis in several organisms (30). These data indicate that PTIP is a transcriptional regulator during embryonic development. Mouse *Ptip* is widely expressed throughout embryogenesis, including when organogenesis begins at embryonic day 8.5 (E8.5) to E10.5 (http://symatlas.gnf.org). *Ptip* null embryos show reduced mitosis and apoptosis beginning at E8.5 and are severely disorganized and dead by E9.5 (5), before possible organogenesis defects can be visualized.

Here, we describe the characterization and positional cloning of two *N*-ethyl *N*-nitrosourea-induced midgestation lethal mutations (*L5Jcs4* and *L5Jcs36*) isolated from a forward genetic screen directed at proximal mouse chromosome 5 (64).

* Corresponding author. Mailing address: Department of Biomedical Sciences, Cornell College of Veterinary Medicine, Ithaca, NY 14853. Phone: (607) 253-3636. Fax: (607) 253-3789. E-mail: jcs92@cornell.edu.

▽ Published ahead of print on 18 August 2008.

The results of positional cloning and complementation studies showed that they are hypomorphic *Ptip* alleles with point mutations in the N- and C-terminal BRCT domains. The hypomorphic nature of these alleles allows mutant embryos to survive longer than null mutants, thus uncovering new aspects of PTIP in vascular formation and extraembryonic development.

MATERIALS AND METHODS

Cell culture. Pooled human umbilical vein endothelial cells (HUVECs) (Lonza, Walkersville, MD) were cultured in EGM2 (Lonza). Mouse embryonic fibroblasts (MEFs) from E9.5 embryos were cultured in Dulbecco's modified Eagle's medium plus 15% fetal bovine serum. Blastocysts were cultured on gelatinized plates in Dulbecco's modified Eagle's medium supplemented with 15% fetal bovine serum, 1.0 mM L-glutamine, 0.1 mM minimal essential medium-nonessential amino acids, 0.1 mM β-mercaptoethanol, and leukemia inhibitory factor. Outgrowths were collected after 6 days of culture for DNA isolation and genotyping.

RNA interference. Small interfering RNA (siRNA) was purchased from Dharmacon (Lafayette, CO), and the sequences were described (24). HUVECs were seeded on six-well plates at 2×10^5 cells/well and grown to 70 to 80% confluence. The cells were then transfected with siRNA against *Ptip* (UGC ACU AGC CUC ACA CAU AdTdT) or scrambled siRNA (CCU ACU AAG CGA CAC CAU UdTdT) at a final concentration of 100 nM using Lipofectamine 2000 (Invitrogen). After 6 h, the transfection medium was replaced with EGM2. The cells were harvested 48 h posttransfection.

Mice, genetic mapping, and complementation testing. The isolation and mapping of *L5Jcs4* and *L5Jcs36* have been described previously (64). For positional cloning, C3HeB/FeJ-*L5Jcs4*/*Rw* females were outcrossed to males that carried the CAST/Ei chromosome 5 semicongenic on the same strain background. *Rw* (rump white) is a visibly marked, recessive lethal inversion. Non-*Rw* F_1-hybrid siblings were intercrossed, and the resulting F_2 offspring were screened for recombination along the *Rw* region by PCR of microsatellite markers polymorphic between C57BL/6J and CAST/EiJ. Primer pairs for "*D5Jcs*" markers are listed in the Mouse Genome Informatics database (informatics.JAX.org).

Complementation testing was performed by crossing *L5Jcs4*/*Rw* to *L5Jcs36*/*Rw* animals. All 18 offspring were *Rw*, indicating that there were no *L5Jcs4*/*L5Jcs36* animals born (six expected; chi square = 9, $P = 0.0027$).

Histological analyses. Deciduae were fixed overnight at 4°C in 4% paraformaldehyde–phosphate-buffered saline (PBS) (137 mM NaCl, 2.7 mM KCl, 4.3 mM Na_2HPO_4, 1.4 mM KH_2PO_4) and then sequentially dehydrated in 50%, 70%, 95%, and 100% ethanol; cleared in xylene; and embedded in paraffin. The sections were 5 μm thick. Feulgen staining was performed as described previously (62). Terminal deoxynucleotidyltransferase-mediated dUTP-biotin nick end labeling (TUNEL) staining was performed with an ApopTag peroxidase in situ apoptosis detection kit (Intergen Co.). VIP (Vector Laboratories) was used as the peroxidase substrate, and counterstaining was performed with 0.5% (wt/vol) methyl green in 0.1 M sodium acetate (pH 4.0).

RNA in situ hybridization and PECAM-1 staining. *Ptip* probes were synthesized by using a DIG RNA labeling kit (primer sequences ATGACCCAGCAG TGGAGATT and GCGACCTCATTTGGTTTCAG; Roche) and hybridized as described previously (63). Embryos for PECAM-1 (platelet-endothelial cell adhesion molecule-1) staining were fixed in 4% paraformaldehyde in PBS overnight at 4°C and stained with a monoclonal anti-PECAM-1 antibody (clone MEC 13.3; Pharmingen). 3,3-Diaminobenzidine (Sigma) was used as the substrate for horseradish peroxidase, using avidin-biotinylated enzyme complex as a signal amplifier (Vector Laboratories). For fluorescent immunodetection, Alexa Fluor 594 goat anti-rat immunoglobulin G (Invitrogen) was used as the secondary antibody.

Quantitative real-time PCR. Amounts of 5 μg of total RNA, from the same preparations used for microarray analysis, were reverse transcribed using a Superscript III system (Invitrogen). ABI TaqMan gene expression assays were used to quantify the expression of *Vegfa*, *Meox2*, and *Stc1*. PCRs were performed on an ABI 7500 real-time PCR system and analyzed with sequence detection software version 1.3 (Applied Biosystems). *Gapdh* was used as the endogenous control for normalization of cDNA input. The relative quantification of gene expression was determined by the $2^{-(\Delta\Delta CT)}$ method (32).

Microarray analysis. E9.5 embryos were dissected from $Ptip^{L5Jcs4}$ intercrosses, and the yolk sacs were harvested for genotyping. Total RNA was isolated using an RNeasy mini kit (Qiagen). The RNA purity and integrity were examined on an Agilent Bioanalyzer 2100. RNA was labeled by using a MessageAmp II-biotin enhanced single-round RNA amplification kit from Ambion (Austin, TX), and cRNA was hybridized to Affymetrix mouse genome 430 2.0 GeneChips and read on a GeneChip scanner 3000 (Affymetrix, Santa Clara, CA). The raw data was processed by using Affymetrix GCOS software to obtain detection calls and signal values. The signals of each array were scaled to a target value of 500 using GCOS software.

Western blot analysis. Protein was extracted from E9.5 embryos or MEFs using radioimmunoprecipitation assay buffer, and the concentration was quantified with a BCA kit (Pierce). Amounts of 15 μg of total protein were separated by sodium dodecyl sulfate-polyacrylamide gel electrophoresis, electrotransferred onto a pure nitrocellulose membrane (Bio-Rad), and probed with the relevant antibodies. Binding was detected by using a Pierce ECL kit. The band intensities were quantified by using NIH Image J software. For the detection of histone components, E9.5 embryos were lysed in TEB (1× PBS containing 0.5% Triton X-100, 2 mM phenylmethylsulfonyl fluoride, and 0.02% NaN_3) on ice for 10 min, pelleted at 2,000 rpm for 10 min at 4°C, washed once with TEB, and resuspended in 0.2 N HCl. After overnight incubation at 4°C, the material was repelleted. Amounts of 3 μg of extracts were separated by using 12% precise protein gels in Tris-HEPES-sodium dodecyl sulfate buffer (Pierce). The antibodies employed were as follows: rabbit anti-PTIP (Bethyl Laboratories); rabbit anti-HIF-1α (Santa Cruz Biotechnology); mouse anti-α-tubulin (Sigma); rabbit anti-cleaved caspase 3 (Cell Signaling); rabbit anti-H4, H3K9M2, -H3K9M3, -H3, -acetyl-H4K12, and -γH2AX (Upstate); and anti-H2Ax, -H3K4M2, -H3K4M3, and -H3K14Ace (Abcam). Chicken anti-PTIP was kindly provided by Gregory Dressler.

Endothelial cell migration and tube formation assay. Cell migration was assessed by a wound healing assay. Two days after siRNA transfection, confluent cultures of HUVECs were scraped with a micropipette tip. The endothelial cell migration from the edge of the injured monolayer was quantified by measuring the distance between the wound edges before and 16 h after incubation. To measure capillary tube formation, HUVECs were seeded on six-well plates at 2×10^5 cells/well. On the following day, the cells were transfected with siRNA against *Ptip* or scrambled siRNA. Forty-eight hours later, the cells were trypsinized and counted. No difference was observed between knockdown and control groups. Amounts of 1×10^4 cells were then seeded on a 96-well plate covered with polymerized ECMatrix (Chemicon) and incubated at 37°C for 12 h in a CO_2 incubator. Images were exported to the Image J program for the identification of endothelial cell tubule-like networks.

RESULTS

Positional cloning of two *Ptip* alleles. As previously reported (64), the *L5Jcs4* and *L5Jcs36* embryonic lethal mutations reside on chromosome 5 within the deletion $Dpp6^{df4J}$ (Fig. 1A). To further narrow the interval, recombination mapping was conducted by intercrossing $L5Jcs4/+^{CAST}$ F_1 heterozygotes and genotyping viable F_2 progeny with microsatellite markers. Regions that were homozygous for the parental (C57BL/6J) markers could not contain the *L5Jcs4* mutation. The recombination mapping data localized *L5Jcs4* to a 966-kb region (between *D5Jcs89* and *D5Jcs75*) containing four RefSeq genes (Fig. 1A). Of these, *Htr5a* and *Dpp6* were eliminated as *L5Jcs4* candidates because homozygous disruptions of them are viable (17, 64). *Speer4b* is a member of a gene family that is expressed in testis specifically (56). Since homozygous knockout of *Ptip* (officially *Paxip1*) causes embryonic lethality (5), this gene was sequenced, revealing a missense mutation (Ser51→Pro) in the N-terminal BRCT domain of PTIP in *L5Jcs4* (Fig. 1B and C). *L5Jcs4* and *L5Jcs36* failed to complement (see Materials and Methods), demonstrating that they are alleles of the same gene. Sequencing uncovered a missense mutation (Leu857→Pro) in the C-terminal BRCT domain of *Ptip* in *L5Jcs36* mice (Fig. 1B and C). Finally, and as shown below, neither *L5Jcs4* nor *L5Jcs36* complemented the lethality of a *Ptip* null allele ($Ptip^-$) (5), proving that *L5Jcs4* and *L5Jcs36* are alleles of *Ptip*. Henceforth, these alleles are designated $Ptip^{L5Jcs4}$ and $Ptip^{L5Jcs36}$.

To determine if the mutations affect PTIP levels or sta-

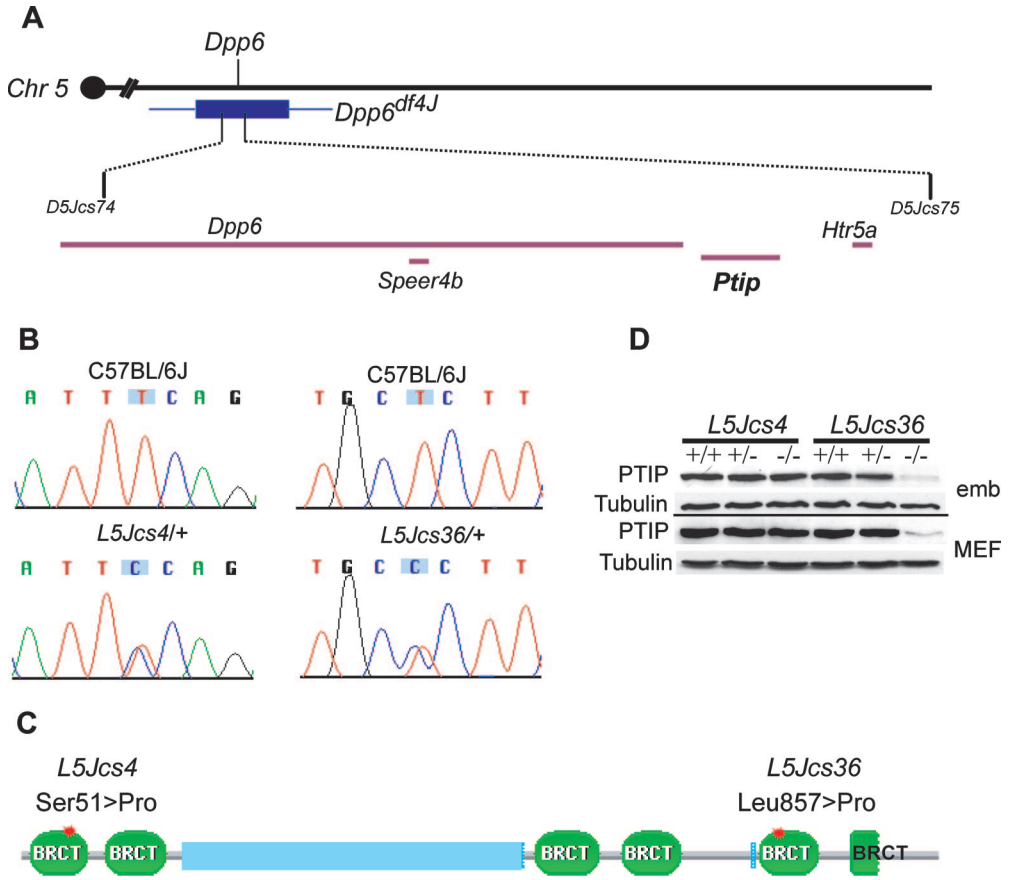

FIG. 1. Genetic mapping and positional cloning of *L5Jcs4* and *L5Jcs36*. (A) Map of the *L5Jcs4* region. The *L5Jcs4* mutation lies within the *Dpp6*^{df4J} deletion (blue bar; the thin lines extending from the bar indicate deletion breakpoint regions), and recombination mapping further refined the critical region as indicated. RefSeq genes within the *L5Jcs4* critical region are shown as purple bars. (B) Identification of missense mutations in *L5Jcs4* and *L5Jcs36* heterozygotes. DNA sequencing traces are shown with mutated bases shaded blue. (C) Schematic structure of mouse PTIP protein, adapted from Pfam. The six BRCT domains and the mutations in PTIP are indicated by the green areas and the red dots, respectively. (D) Western blot of PTIP protein in E9.5 embryos (emb) and MEFs. Duplicate blots were probed with anti-α-tubulin as a loading control. The predicted PTIP protein is 130 kDa.

bility, Western blot analysis of protein extracted from E9.5 embryos and MEFs was performed. Whereas PTIP levels in *Ptip*$^{L5Jcs4/L5Jcs4}$ samples were indistinguishable from the levels in controls, there was markedly decreased PTIP in *Ptip*$^{L5Jcs36/L5Jcs36}$ embryos and MEFs (Fig. 1D). The reduction in PTIP protein was not accompanied by decreased mRNA levels (data not shown). Therefore, the mutated C-terminal BRCT domain of PTIP^{L5Jcs36} apparently renders it unstable or more susceptible to degradation.

***Ptip*^{L5Jcs4} and *Ptip*^{L5Jcs36} are hypomorphic *Ptip* alleles.** To characterize the timing and nature of the embryonic lethality, we analyzed the morphology of mutant embryos at different stages of gestation. At E9.5, *Ptip*^{L5Jcs4} homozygotes were smaller than their wild-type (WT) siblings, but the gross morphology, including the head, heart, and trunk, did not show obvious abnormalities (Fig. 2B). However, *Ptip*^{L5Jcs36} mutants were severely growth retarded. They had shortened trunks and poorly developed headfolds, and they failed to complete embryonic turning and heart looping (Fig. 2C). Consistent with the first two phenotypes, the results of RNA in situ hybridization revealed that *Ptip* transcripts are most abundant in the brain and posterior regions at E8.5 (Fig. 2K). *Ptip*$^{-/-}$ embryos were disorganized and degenerating at E9.5 (Fig. 2D). At E10.5, the most striking feature of *Ptip*$^{L5Jcs4/L5Jcs4}$ embryos, aside from the smaller size, was a swollen pericardial sac (Fig. 2F). At this stage, *Ptip*$^{L5Jcs36/L6Jcs36}$ embryos had a pale color, were disorganized, and were degenerating. All *Ptip*^{L5Jcs36} mutants had a failure of chorioallantoic fusion (Fig. 2G). *Ptip*$^{-/-}$ embryos were undergoing resorption by E10.5 (Fig. 2H). With death characterized by tissue degeneration and lack of a beating heart, *Ptip*$^{L5Jcs4/L5Jcs4}$, *Ptip*$^{L5Jcs36/L5Jcs36}$, and *Ptip*$^{-/-}$ embryos died at E12.5, E10.5, and E9.5, respectively. The results indicate that *Ptip*^{L5Jcs4} is a milder allele than *Ptip*^{L5Jcs36}, which in turn is less severe than the null. The hypomorphic nature of *Ptip*^{L5Jcs4} and *Ptip*^{L5Jcs36} was also supported by the phenotypic resemblance of *Ptip*^{L5Jcs4}/*Ptip*$^{-}$ and *Ptip*^{L5Jcs36}/*Ptip*$^{-}$ compound mutant embryos to the corresponding missense homozygotes (Fig. 2I and J).

***Ptip*^{L5Jcs4} and *Ptip*^{L5Jcs36} cause defects in vascular formation.** At E9.5, all *Ptip*^{L5Jcs4} homozygotes were growth retarded, but only ~40% of embryos had an inflated pericardium. To explore if the cardiac defect is secondary to a failure in vasculogenesis, whole-mount embryos were stained with the pan-vessel-specific marker PECAM-1. Unlike control siblings,

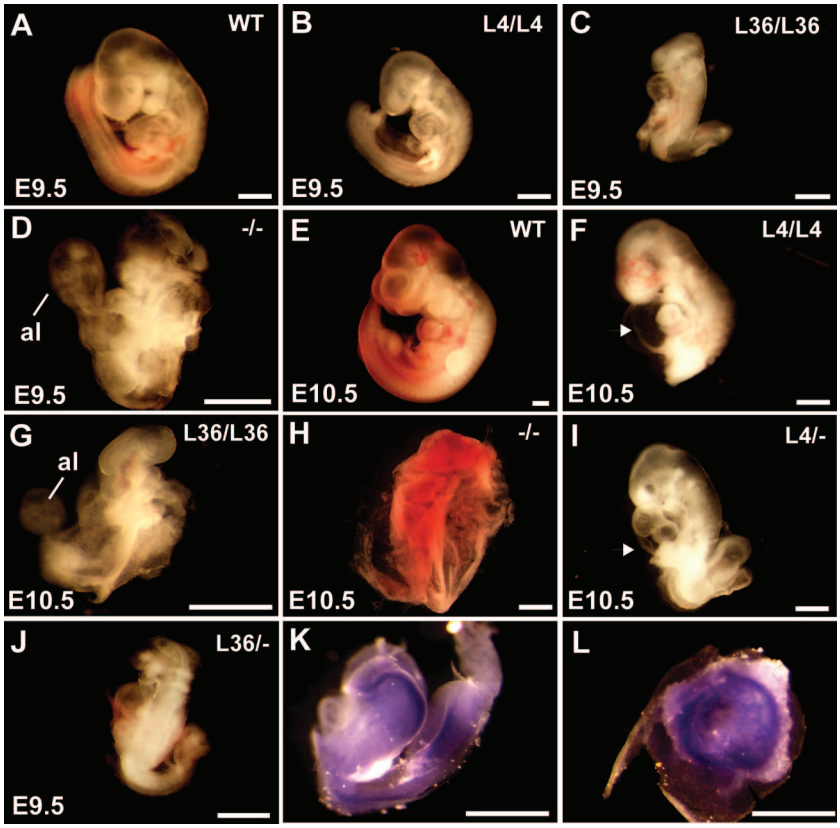

FIG. 2. *Ptip*^{L5Jcs4} and *Ptip*^{L5Jcs36} are hypomorphic *Ptip* alleles. Shown are whole-mount embryos at indicated gestational ages and genotypes (L4, *Ptip*^{L5Jcs4}; L36, *Ptip*^{L5Jcs36}; −, *Ptip* knockout allele). Arrowheads in panels F and I highlight the enlarged pericardia. The defective allantois ("al") is indicated in panels D and G. Panel H shows a yolk sac. (K, L) In situ hybridization of antisense *Ptip* RNA to WT E8.5 embryo and chorionic placenta, respectively. Size bars = 500 μm.

Ptip$^{L5Jcs36/L5Jcs36}$ embryos had a deficiency of blood vessels throughout their bodies (Fig. 3E and F). *Ptip*$^{L5Jcs4/L5Jcs4}$ embryos did not show vascular formation defects at E9.5 (data not shown). However, angiogenesis impairment was obvious in E10.5 *Ptip*^{L5Jcs4} homozygotes. Blood vessel networks failed to elaborate properly in the head (Fig. 3B). In somitic regions, there was a lack of small sprouting blood vessels compared to the blood vessel development in controls (Fig. 3C and D). In WT littermates, aortic arches were visible and connected with the dorsal aorta (Fig. 3A), whereas a well-developed aortic arch was not formed in the *Ptip*^{L5Jcs4} mutants (Fig. 3B). To rule out the possibility that the vasculogenesis and developmental abnormalities in *Ptip*^{L5Jcs4} and *Ptip*^{L5Jcs36} mutants (Fig. 2 and 3) were due to a generalized failure of mesoderm formation, we examined the expression of Brachyury (*T*) by in situ hybridization in E8.5 and E9.5 embryos. *T* expression appeared normal in the mutants (Fig. 4). However, because *Ptip*$^{L5Jcs36/L5Jcs36}$ embryos show caudal truncation, it is possible that there is an impairment in the continual supply of mesoderm.

PTIP dysfunction impairs extraembryonic tissue development. Yolk sac defects and placental insufficiency are two primary causes of embryonic lethality in midgestation (E8.5 to E12.5) embryos (43). E10.5 WT yolk sacs exhibited hierarchically organized vessel architecture with numerous large blood-filled vitillene vessels (Fig. 5A). In contrast, the yolk sacs of *Ptip*$^{L5Jcs4/L5Jcs4}$ embryos were pale and lacked prominent vasculature (Fig. 5B). Whole-mount PECAM-1 staining of yolk sacks further revealed the lack of a properly developed capillary network or branching of large vessels (Fig. 5C to F). Histological analysis revealed dense, large blood vessels filled with primitive nucleated blood cells in E9.5 controls (Fig. 5G). In contrast, the blood vessel diameters in *Ptip*^{L5Jcs4} and *Ptip*^{L5Jcs36} mutants were smaller (Fig. 5H and I) and there were fewer blood vessels in the latter.

The vascular portion of the placenta is derived from extraembryonic mesoderm (allantois) that extends from the posterior end of the embryo at E8.0. At E8.5, the allantois and the chorion fuse in a process called chorioallantoic attachment. Soon thereafter, the chorion folds to form villi, creating a space into which the fetal blood vessels grow from the allantois (7). The abnormal allantois in *Ptip*$^{L5Jcs36/L5Jcs36}$ embryos led to failure of chorioallantoic attachment (Fig. 2G). Although chorioallantoic attachment occurred in *Ptip*^{L5Jcs4} mutants, the chorion-derived labyrinth layer was much smaller than in WT littermates and was less defined (Fig. 5J and K). *Ptip* expression is abundant in the chorion (Fig. 2L).

***Ptip* mutation causes deregulation of angiogenesis genes.** PTIP physically interacts with transcription factors and is a component of a histone methyltransferase complex (22, 44), suggesting the involvement of PTIP in transcriptional regulation. Therefore, we investigated the impact of the *Ptip*^{L5Jcs4} mutation on gene expression during embryogenesis by mi-

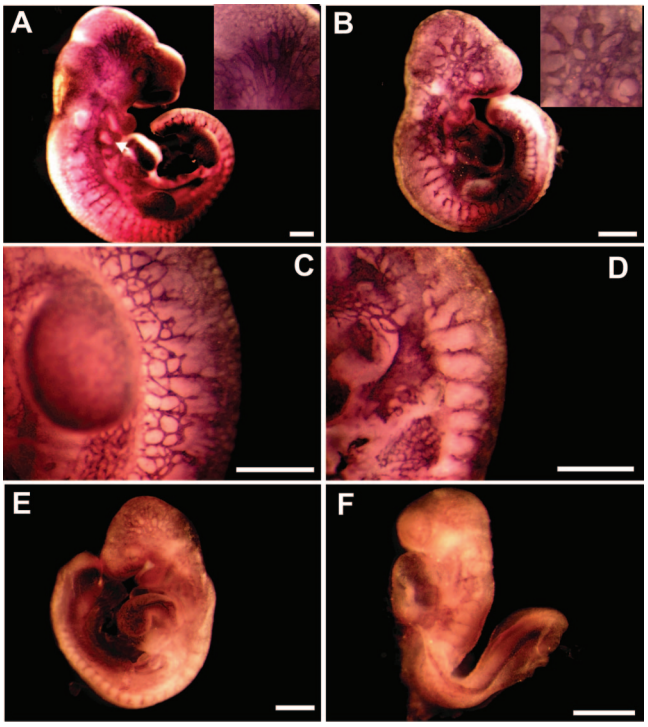

FIG. 3. Vascular defects in *Ptip* mutants. Shown are whole-mount embryos stained with PECAM-1. (A to D) E10.5 embryos. (A) In WT littermates of $Ptip^{L5Jcs4}$ mutants, the head contains large, fused blood vessels (inset). (B) In $Ptip^{L5Jcs4}$ mutants, the blood vessels are not remodeled properly (inset). The arrowhead in panel A points to aortic arches, which are missing in $Ptip^{L5Jcs4}$ mutants. (C, D) Vascular formation in somite regions. (C) WT littermate of $Ptip^{L5Jcs4}$ mutants. (D) In $Ptip^{L5Jcs4}$ mutants, there is a lack of small sprouting vessels. (E, F) E9.5 embryos. (E) WT littermate of $Ptip^{L5Jcs36}$ mutants. (F) In $Ptip^{L5Jcs36}$ mutants, blood vessels are sparse. Size bars = 500 μm.

croarray analysis of mutant and WT E9.5 embryos. This revealed 298 differentially expressed genes, of which 58 had a >50% change ($P < 0.01$). Among these 58 genes, 14 were reduced in $Ptip^{L5Jcs4/L5Jcs4}$, and 44 were increased (Fig. 6A).

To identify possible relationships among the 58 differentially expressed genes, network analysis was performed using the Ingenuity database and software (www.ingenuity.com). This revealed one network of 15 genes containing the critical regulator of vasculogenesis, VEGF, at its core (Fig. 6B). The results of quantitative PCR verified the upregulation of VEGFA in $Ptip^{L5Jcs4/L5Jcs4}$ embryos (Fig. 6D), and the results of semiquantitative reverse transcription-PCR indicated that all three isoforms of mouse VEGFA were elevated in the mutant (Fig. 6C). To exclude the possibility that VEGFA upregulation is secondary to impaired blood circulation and consequent hypoxia, the levels of HIF-1α, which is induced and promotes *Vegfa* transcription under hypoxic conditions (50), were assessed by immunoblotting. No difference in HIF-1α was found between WT, $Ptip^{L5Jcs4/L5Jcs4}$, and $Ptip^{L5Jcs36/L5Jcs36}$ embryos (Fig. 6E). In the VEGFA network, *Meox2* and *Stc1* are also implicated in angiogenesis. *Meox2* heterozygous mutants have an ~50% reduction in total brain capillary length (65). STC1 may play a selective modulatory role in angiogenesis, possibly serving as a "stop" signal or stabilizing factor contributing to the maturation of newly formed blood vessels (68). The alterations in *Meox2* and *Stc1* expression levels were also confirmed by quantitative real-time PCR (Fig. 6D). These combined data suggest that PTIP is associated with angiogenesis signaling pathways.

***Ptip* knockdown impairs endothelial cell migration and capillary tube-like formation.** Angiogenesis is regulated by a tight balance between pro- and antiangiogenic agents. It involves a cascade of events, of which capillary endothelial cell migration is an essential component (27). To investigate whether the angiogenesis defects in the hypomorphic *Ptip* alleles are caused by dysfunction of endothelial cells, we performed siRNA knockdown of PTIP in HUVECs and observed the effects on cell migration and capillary tube-like formation. The results of Western blot analysis showed that PTIP protein was reduced >80% in siRNA-transfected HUVECs compared to its level in scrambled siRNA controls (Fig. 7A and B). The results of a wound healing assay showed that the migration rate of the knockdown cells was only 40% of the migration rate of controls (Fig. 7C and D). In vitro culture of HUVECs on Matrigel can mimic sprouting and tube formation during angiogenesis in vivo (46). Figure 7E illustrates the markedly reduced tubule formation in PTIP knockdown cells compared to the tubule formation in controls. Quantification of the results of multiple experiments indicated that both the length of the tubule structures and the number of branch points were reduced in the siRNA-treated cells (Fig. 7F and G). Although no decrease in cell number was observed 48 h after *Ptip* siRNA treatment (not shown; see Materials and Methods), there was an increase in cleaved caspase 3 (Fig. 7H). In the results of similar assays, decreased tube formation and cell migration were associated with increased apoptosis in cells conditionally inactivated (by Cre-recombinase) for focal adhesion kinase (52). Thus, increased apoptosis may have a role in the vascular formation defects in *Ptip* mice.

Knockdown of MLL, an H3K4 methyltransferase, impaired the migration and sprout formation of umbilical endothelial cells, suggesting a role of histone methylation in regulating angiogenic function (9). Since PTIP is a component of a histone H3K4 methyltransferase complex (44), alteration in histone H3K4 methylation due to PTIP dysfunction might result in the observed deregulation of angiogenesis genes described earlier. However, we did not observe a decrease in H3K4 di- or trimethylation (or several other histone modifications) in the results of Western blot analysis of protein from E9.5 embryos (Fig. 8A), in contrast to the results of in situ studies of knockout embryos that reported global decreases (44). Furthermore, siRNA-mediated knockdown of *Ptip* in HUVECs did not alter the levels of H3K4 di- or trimethylation (Fig. 8B).

The essential roles of PTIP in embryogenesis are not attributable to apoptosis or generalized defects in cell proliferation. To determine if the lethality of mutant embryos is a consequence of generalized cellular dysfunction, we examined apoptosis levels by both TUNEL staining and Western blot analysis of cleaved caspase 3. Additionally, we assessed cell proliferation in MEF cultures and by blastocyst outgrowth assays. Compared to those of WT littermates (Fig. 9A), histological sections of E9.5 $Ptip^{L5Jcs4/L5Jcs4}$ embryos did not indicate elevated apoptosis (Fig. 9B and F) or an activated caspase 3 pathway (Fig. 9E), while $Ptip^{L5Jcs36/L5Jcs36}$ embryos showed

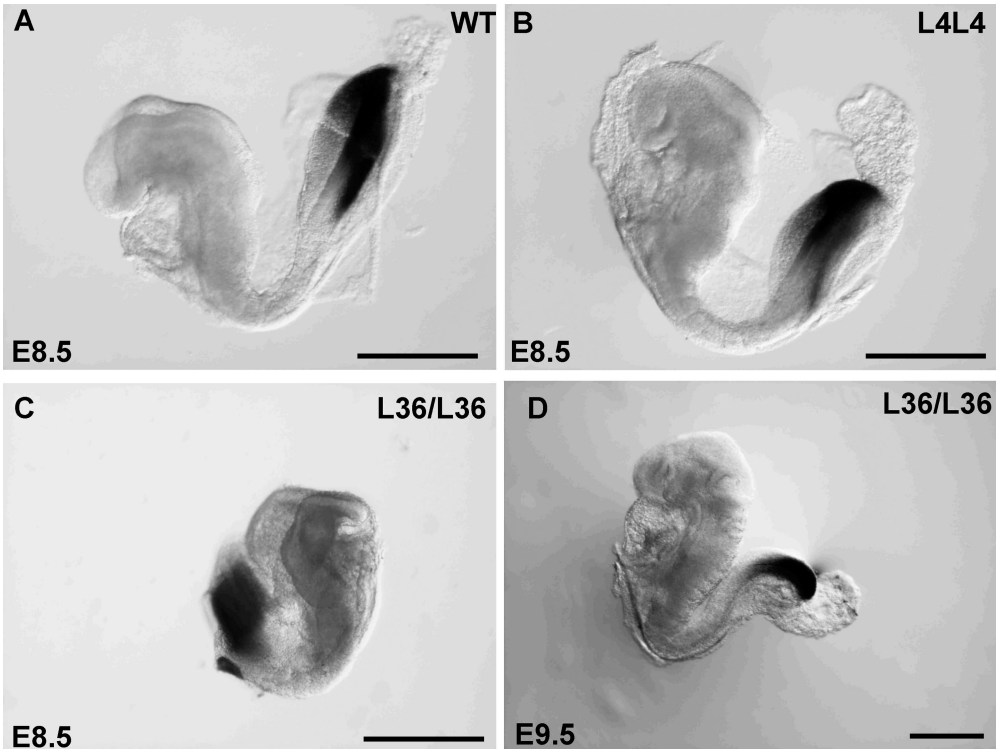

FIG. 4. Brachyury expression in embryos. An antisense Brachyury (*T*) riboprobe was hybridized to whole embryos of the indicated gestational ages. Note that the E9.5 embryo in panel D has the developmental appearance of an E8.5 embryo (failed to undergo turning) due to the mutation. L4, $Ptip^{L5Jcs4}$; L36, $Ptip^{L5Jcs36}$. Size bars = 500 μm.

increases in both (Fig. 9C to F). Since $Ptip^{L5Jcs36}$ mutants experience severe vasculogenesis defects at E9.5, we surmise that this enhanced apoptosis is a secondary consequence of decreased blood supply. $Ptip^{L5Jcs4/L5Jcs4}$ (not shown) and $Ptip^{L5Jcs36/L5Jcs36}$ blastocysts were able to attach to culture plates, and their inner cell masses proliferated as did those of WT controls (Fig. 9G and H). Similarly, MEFs of these genotypes propagated for >5 passages in vitro (data not shown). These results indicate that PTIP has specific cellular functions during embryogenesis but that these hypomorphic alleles are not required for general cell proliferation.

PTIP-deficient cells do not exhibit hypersensitivity to spontaneous DNA damage, but mutation of the C-terminal BRCT domain causes moderate sensitivity to induced DSBs. BRCT domains are most often found in proteins involved in DNA repair and cell cycle checkpoint control. These functions are particularly important during early embryogenesis, when cell proliferation and DNA replication are highly active. PTIP was reported to participate in a DNA damage response induced by double-strand break (DSB)-inducing agents (5, 24, 34). Therefore, to determine if PTIP deficiency causes excessive spontaneous genome damage, we examined the frequency of chromosomal aberrations in metaphase spreads prepared from *Ptip* mutant MEFs (Fig. 10A). No chromosome abnormalities were detected in 60 spreads from each mutant genotype tested.

Phosphorylation of H2AX (33) and acetylation of H4 (41) occur on damaged DNA and are biomarkers for assessing DNA damage levels in cells. In mutant E9.5 embryos, no increase in these two modified proteins was detected by Western blot analysis (Fig. 10B). The results of other studies have shown that PTIP is involved in the response to stress-induced DNA damage (5, 24). Consistent with these reports, we found that $Ptip^{L5Jcs36/L5Jcs36}$ MEFs had increased sensitivity to the DSB-inducing agents camptothecin and ionizing radiation (Fig. 10C). The response of PTIP to DNA damage, including its recruitment to DNA damage foci and interaction with 53BP1, occurs via its C-terminal BRCT domain, which is disrupted in $Ptip^{L5Jcs36}$. $Ptip^{L5Jcs4/L5Jcs4}$ MEFs did not have significantly elevated sensitivity to DNA damage, indicating that the N-terminal BRCT domain (which is mutated in this allele) has a role in embryonic development, but not in DNA damage responses.

DISCUSSION

PTIP plays essential but poorly understood roles in mouse embryonic development. The results of a previous study suggested that this protein is required for cell proliferation (5). Using the two hypomorphic PTIP alleles obtained by a forward genetic screen, we uncovered novel functions of this protein in embryonic vascular formation and extraembryonic tissue development. Defects in the cardiovascular system and extraembryonic tissues appear to be the primary causes of embryonic lethality in the two hypomorphic *Ptip* mutants we describe.

TGFβ signaling controls cell proliferation, cell recognition, differentiation, apoptosis, and specification of developmental fate in species ranging from flies to mammals (53). Smad family proteins lie at the core of this signaling pathway and

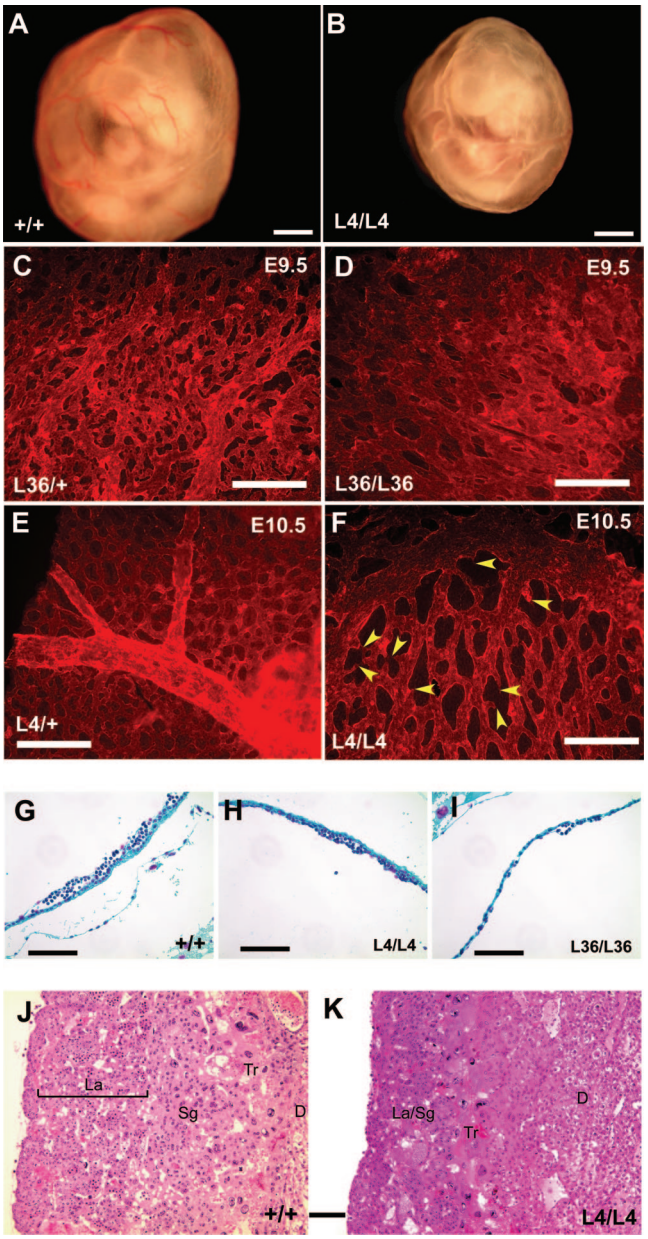

FIG. 5. Extraembryonic tissue abnormalities in $Ptip^{L5Jcs4}$ and $Ptip^{L5Jcs36}$ mutant embryos. (A, B) Whole-mount yolk sacs at E10.5. The $Ptip^{L5Jcs4}$ (L4) mutant (B) has sparse blood vessels compared to the WT (+/+) control (A). Size bars = 500 μM. (C to F) PECAM-1-stained whole-mount yolk sacs. The genotypes and gestational ages are indicated. Size bars = 200 μM. Dense capillary networks and maturing, large, branching vessels are evident in controls (C, E), but the mutants (D, F) are not well developed. (F) The $Ptip^{L5Jcs4}$ mutant yolk sac displays a number of incomplete sprouts, indicated by arrowheads. (G to I) Feulgen-stained sections of E9.5 yolk sacs from WT, $Ptip^{L5Jcs4}$, and $Ptip^{L5Jcs36}$ embryos, respectively. (J, K) Hematoxylin and eosin-stained sections of E10.5 placentas of WT (J) and mutant (K) embryos. D, decidua; Tr, trophoblast giant cells; Sg, spongiotrophoblast; La, labyrinth layer. In the mutant, the labyrinth and spongiotrophoblast layers are difficult to discern and are smaller, in aggregate, than in the WT. Size bars = 100 μm.

regulate the expression of genes involved in embryonic development. A connection between PTIP and TGFβ-Smad signaling has been demonstrated in *Xenopus*. Inhibition of SWIFT, the *Xenopus* ortholog of mammalian PTIP, results in the suppression of TGFβ-induced gene transcription and defective trunk development (54), the latter of which occurs in $Ptip^{L5Jcs36}$ mutants. SWIFT physically interacts with Smad1/Smad2 and activates target gene transcription in a TGFβ-dependent manner. Since the BRCT domains of PTIP and SWIFT are 80% identical and there is >95% identity between mouse and *Xenopus* Smad1/Smad2, it is likely that the functions of vertebrate PTIP during embryogenesis are conserved. Knockout of TGFβ signaling pathway components, including the ligand (*Tgfβ1*) (8), receptors (*Alr1* and *Alr5*) (28, 42, 60), and effectors (*Smad1*, *Smad2*, and *Smad5*) (4, 20, 29, 59, 66), causes lack of normal vasculature in the yolk sac, marked impairment of allantois formation, failure of embryonic turning and anterior morphogenesis, or defects in embryonic vascular formation. We found that the regions of highest *Ptip* expression, such as brain, posterior streak, and chorion, showed obvious developmental defects in the hypomorphic alleles.

The anatomic characterization, gene expression profiling, and in vitro angiogenesis data presented here demonstrate that PTIP is involved in vasculogenesis and angiogenesis during embryogenesis. Our data lead us to hypothesize that deregulation of *Vegfa* underlies these defects in *Ptip* mutants. VEGFA is a crucial regulator of vascular development during embryogenesis, participating in the specification of blood islands and the proliferation, survival, and migration of endothelial cells. Proper VEGFA levels are tightly controlled during angiogenesis. The loss of a single VEGFA allele in mice causes embryonic lethality at E9 due to cardiovascular defects (3, 11), while the overexpression of VEGFA induces embryonic cardiac failure (39) and impaired retinal vascular patterning (40). In zebrafish, the *Vegfa* promoter contains a number of bone morphogenetic protein-activated Smad binding elements (SBEs), implicating Smad1 and Smad5 in the regulation of bone morphogenetic protein-induced *Vegfa* expression (18). In mouse macrophages, two SBEs are critical for TGFβ1-induced *Vegf* promoter activity (23). Since *Vegfa* transcription increases in the *Ptip* mutants, perhaps PTIP interaction with Smads inhibits their ability to bind the SBEs. Alternatively, PTIP may recruit a negative regulator to the *Vegf* promoter, via sequence-specific binding driven by Smads (see below). The mechanism by which *Vegf* is upregulated by the absence of PTIP requires further investigation.

Although it was reported that PTIP is a component of a histone H3K4 methyltransferase complex and knockout embryos exhibited markedly decreased H3K4 di- and trimethylation by in situ analysis (44), we did not observe a decrease in H3K4 di- or trimethylation (or any of several other histone modifications) in Western blot analysis of protein from E9.5 $Ptip^{L5Jcs4}$ or $Ptip^{L5Jcs36}$ mutant embryos (Fig. 8A). One explanation for this disparity may be that the BRCT domain mutations do not affect binding of the hypomorphic *Ptip* alleles to PAX2, which promotes H3K4 methyltransferase complex formation at specific sites (44). However, this would necessitate that the reduced $PTIP^{L5Jcs36}$ levels are sufficient for complex formation. Also, PTIP knockdown inhibited HUVEC migration and capillary tube formation but did not reduce H3K4 methylation (Fig. 8B) or affect the expression of the genes regulated by this histone modification (data not shown). Perhaps our observations reflect a cell type difference in PTIP's

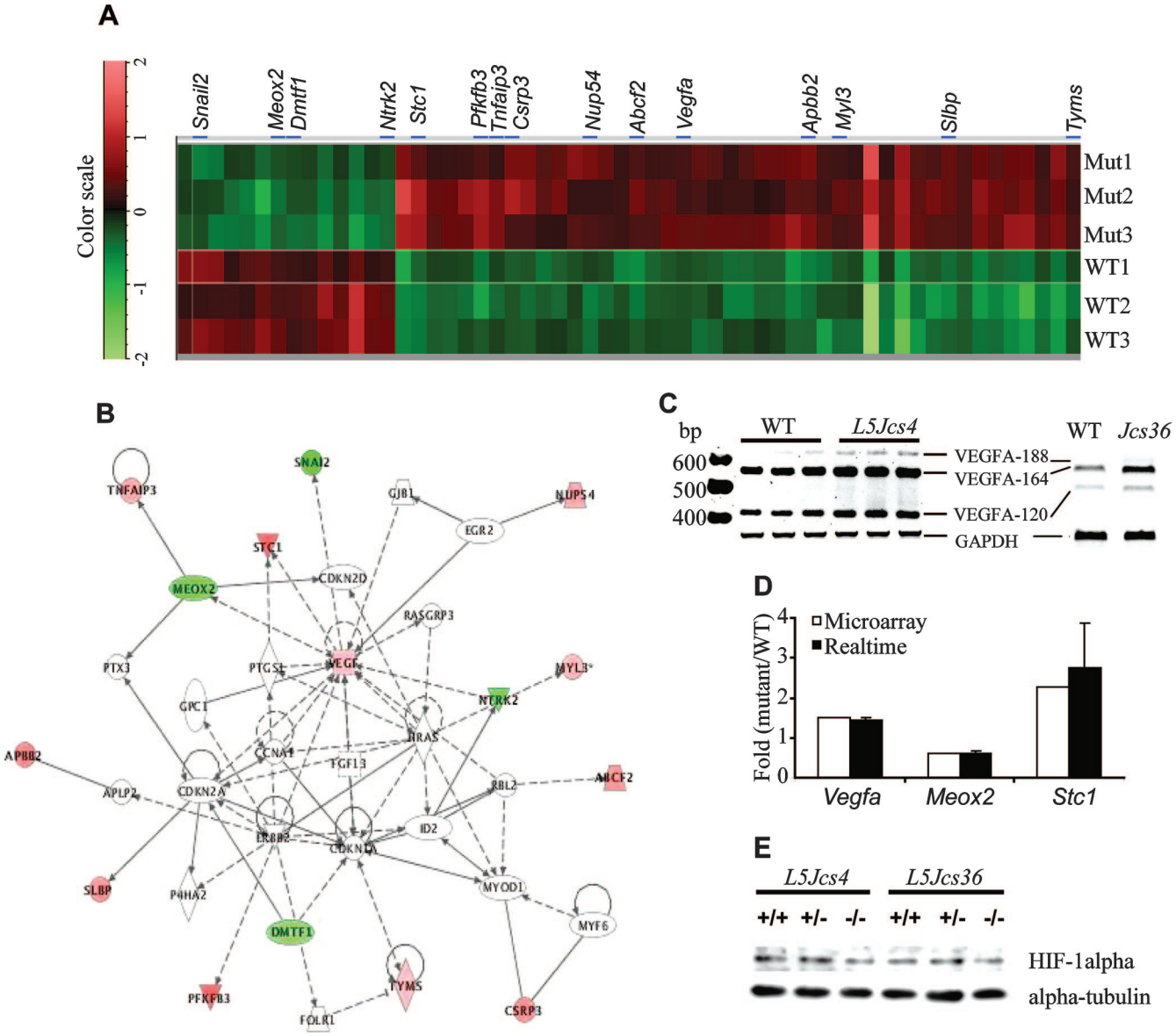

FIG. 6. Gene expression profiling of *Ptip* mutants. (A) Cluster analysis of the top 58 differentially expressed genes. Each has a >50% change from the WT. Genes were clustered in columns, with each array experiment in a row. The 15 genes included in the VEGF gene network are indicated by blue bars and are listed above the heat map. Red equals upregulation, and green equals downregulation. (B) Gene network analysis of 58 differentially expressed genes. The genes shaded pink (induced expression) and green (repressed expression) are PTIP dependent. (C) Reverse transcription-PCR analysis of *Ptip* isoforms in E9.5 embryos. GAPDH (glyceraldehyde-3-phosphate dehydrogenase) was used as a control. (D) Quantification of *Vegfa*, *Meox2*, and *Stc* expression by real time PCR. Error bars show standard errors of the means. (E) Western blot analysis of HIF-1α in E9.5 embryos. The same blot was probed with anti-α-tubulin.

role in chromatin modification. Patel et al. noted decreased H3K4 methylation in presumptive neural tissues of the headfolds and mesodermal derivatives of E9 embryos, but not in extraembryonic tissues (44).

PTIP is associated with active chromatin but does not itself possess transactivation activities (30). The results of transient transfection studies revealed that PTIP is a strong inhibitor of the transactivation activities of PAX2A and PAX2B on the glucagon promoter. The binding of p8, a nuclear DNA binding protein, to PTIP prevents this inhibition (21). PTIP might also interact with CCAAT/enhancer-binding proteins (C/EBP) via phosphoserine-containing motifs localized in a highly conserved region of C/EBP transactivation domains (38). The transactivation domain regions of PAX and C/EBP contain a PTIP binding motif, suggesting that PTIP may serve as a transcriptional coregulator.

As discussed above, PTIP could regulate embryonic development via TGFβ/Smad signaling pathways. The transcriptional regulatory activity (both positive and negative) and specificity of Smad proteins are regulated by Smad complex cofactors that affect SBE binding affinity (36). PTIP contains six BRCT domains which provide multiple binding sites for its

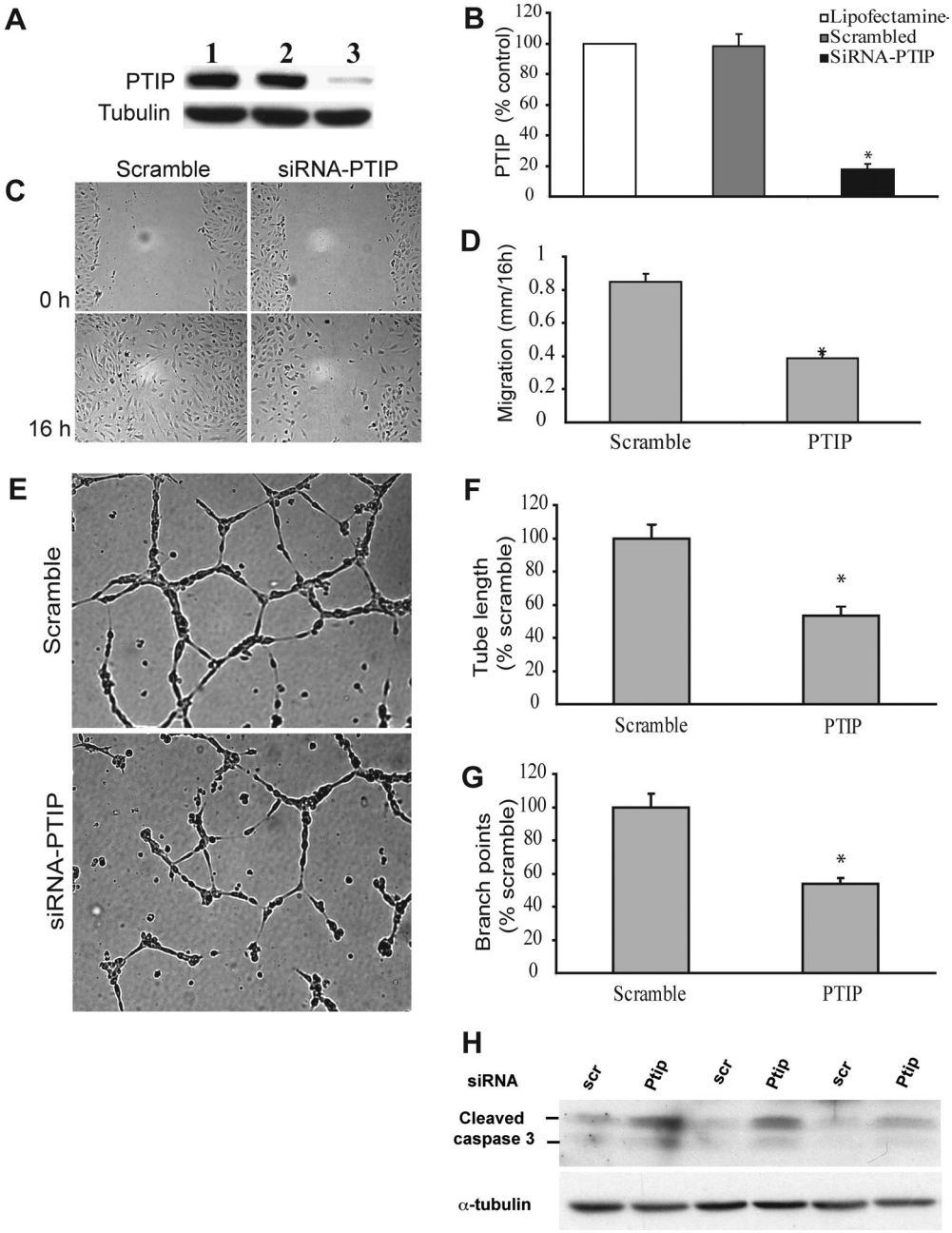

FIG. 7. PTIP regulates endothelial cell migration and tube formation. (A, B) HUVECs were transfected with siRNA complementary to *Ptip* or with double-stranded RNA containing scrambled versions of the complementary siRNA and then cultured for 48 h. (A) Proteins were extracted for Western analysis with the indicated antibodies. Lanes: 1, mock transfected; 2, scrambled siRNA; 3, siRNA-*Ptip*. (B) Quantification of band intensities (% of control values) is shown as means ± standard errors of the means (SEM) ($n = 3$; *, $P < 0.05$). (C, D) Endothelial cell migration after a scratch wound 48 h after siRNA transfection. (D) Quantification of the data as means ± SEM ($n = 10$; *, $P < 0.05$), as described in Materials and Methods. (E to G) Tube formation assay in siRNA-treated HUVECs. Images of representative fields are shown. The lengths of tubes (F) and the numbers of branch points (G) were quantified (% of control values) from the results of five independent experiments and are shown as the means ± SEM. *, *P* value is <0.05 versus the result for scrambled siRNA. (H) Assessment of apoptosis in *Ptip* knockdown HUVEC cells by Western blot analysis of cleaved caspase 3. The cells (three replicates) were harvested for protein extraction 48 h after siRNA treatment. scr, scrambled siRNA.

interacting partners (14). We propose that PTIP participates in the organization of transcriptional complexes via the recruitment of transcription factor cofactors at promoters, thereby controlling the specificity and activity of gene expression during embryogenesis.

The four C-terminal tandem BRCT domains of PTIP are required for mediating the response to DSBs. The function of the N-terminal BRCT domains is unknown. The mutation of an N-terminal BRCT domain in *Ptip*^{L5Jcs4} did not impair PTIP stability or the response to radiation-induced DNA damage,

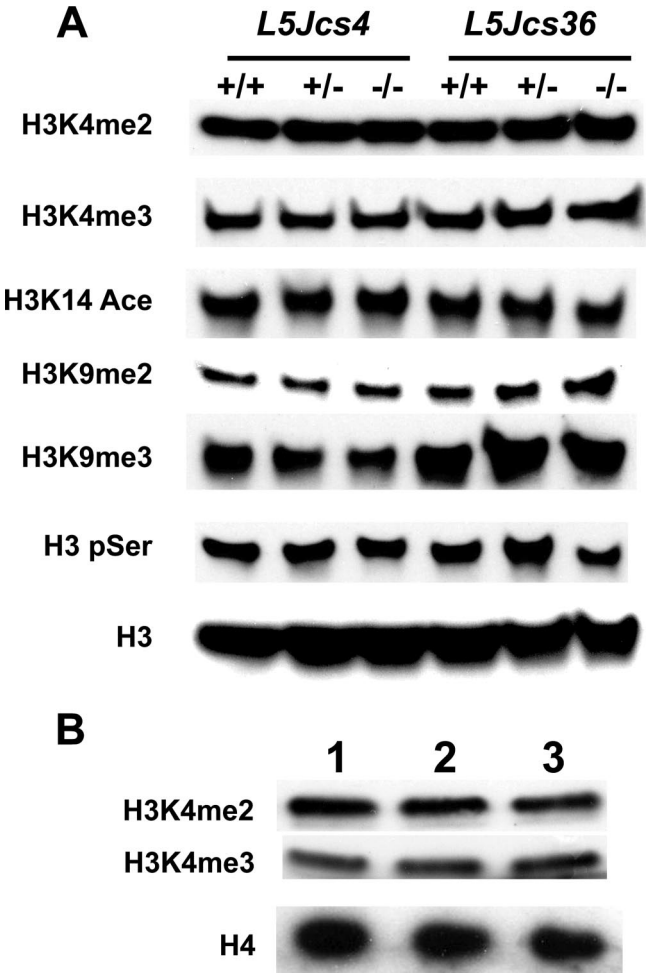

FIG. 8. Western blot analysis of histone H3 modifications. (A) Protein from E9.5 embryos probed with the indicated antibodies. Anti-pan-H3 served as a loading control. (B) HUVECs were transfected with siRNA complementary to *Ptip* or with double-stranded RNA containing scrambled versions of the complementary siRNA and then cultured for 48 h. Extracted proteins were probed with the indicated antibodies. Lanes: 1, mock transfected; 2, scrambled siRNA; 3, siRNA-*Ptip*. Anti-pan-H4 served as a loading control.

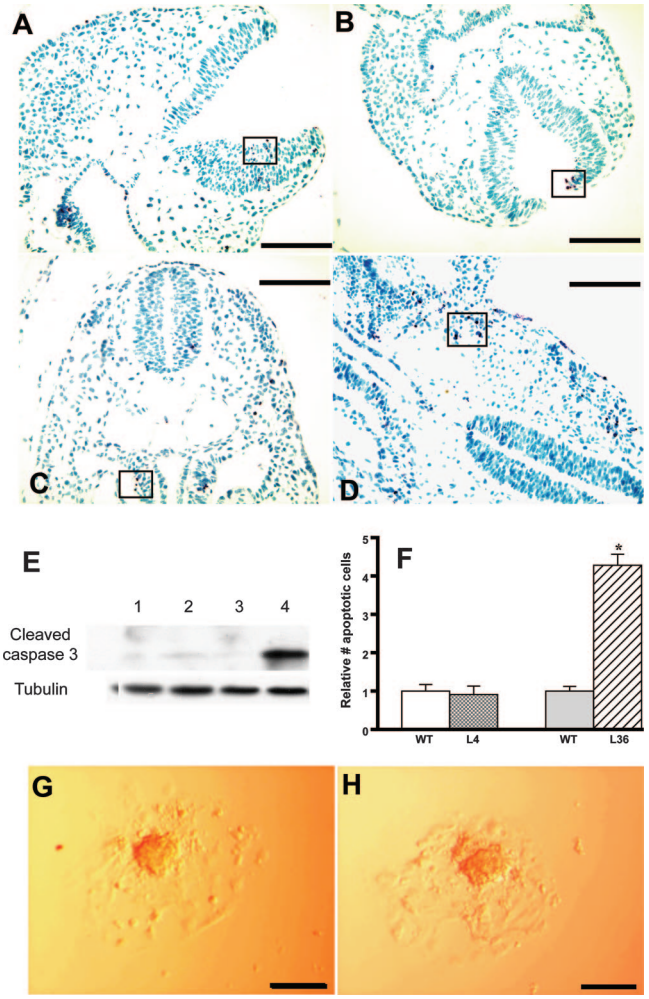

FIG. 9. Apoptosis and cell proliferation in *Ptip* mutants. (A to D) TUNEL-stained paraffin sections of E9.5 embryos. WT littermate of $Ptip^{L5Jcs4}$ mutants (A); $Ptip^{L5Jcs4}$ mutant (B); WT littermate of $Ptip^{L5Jcs36}$ mutants (C); $Ptip^{L5Jcs36}$ mutant (D). TUNEL-positive apoptotic cells are darkly stained compared to the methyl green-counterstained cells. In each panel, selected clusters of apoptotic cells are enclosed in a rectangle. (E) Western blot analysis of cleaved caspase 3, a marker for apoptosis. Lanes: 1, WT littermate of $Ptip^{L5Jcs4}$ mutants; 2, $Ptip^{L5Jcs4}$ mutant; 3, WT littermate of $Ptip^{L5Jcs36}$ mutants; 4, $Ptip^{L5Jcs36}$ mutant. (F) Quantification of apoptotic cells in TUNEL-stained sections. For each genotype, apoptotic cells from eight whole-embryo sections were counted, and the number is represented as a relative value (controls were set at 1). Error bars show standard errors of the means. *, $P = 0.0001$; L4, $Ptip^{L5Jcs4}$; L36, $Ptip^{L5Jcs36}$. (G, H) Inner cell mass outgrowths of WT (G) and $Ptip^{L5Jcs36}$ mutant (H) blastocysts after 6 days in culture. The size bars in panels A to D and panels G and H indicate 100 μm and 300 μm, respectively.

suggesting that this mutation might only disturb the conformation of the N-terminal BRCT domains. Therefore, $Ptip^{L5Jcs4}$ may be a separation-of-function allele that is useful for dissecting the essential physiological roles of PTIP mediated through the N-terminal BRCT domains. Since the $Ptip^{L5Jcs36}$ C-terminal BRCT domain mutation severely reduces the amount of PTIP, we do not know if these BRCT domains are required for embryogenesis. Given the binding of *Xenopus* PTIP/Swift to Smad2 via C-terminal BRCT domains (54), the N- and C-terminal BRCT domains might cooperate to interact with molecules involved in embryonic processes.

Although mouse PTIP was first identified by its physical interaction with Pax family proteins, it is unclear whether the essential roles of PTIP in embryogenesis are linked with Pax during organogenesis. Among nine Pax family members in mice, only the deletion of *Pax3* caused embryonic lethality, due to defective cardiac neural crest migration and consequent malformation of cardiac outflow tracts (6). The other Pax mutants were not demonstrated to undergo defects in vasculogenesis and extraembryonic tissue, as shown in *Ptip* mutants, suggesting that the roles of PTIP during early embryonic development are mediated via interactions with other developmental regulators. However, Pax family proteins might share some redundancy (35) or function synergistically (45) in organogenesis. Provided that PTIP interacts with more than one Pax member in specific tissues, the loss of PTIP

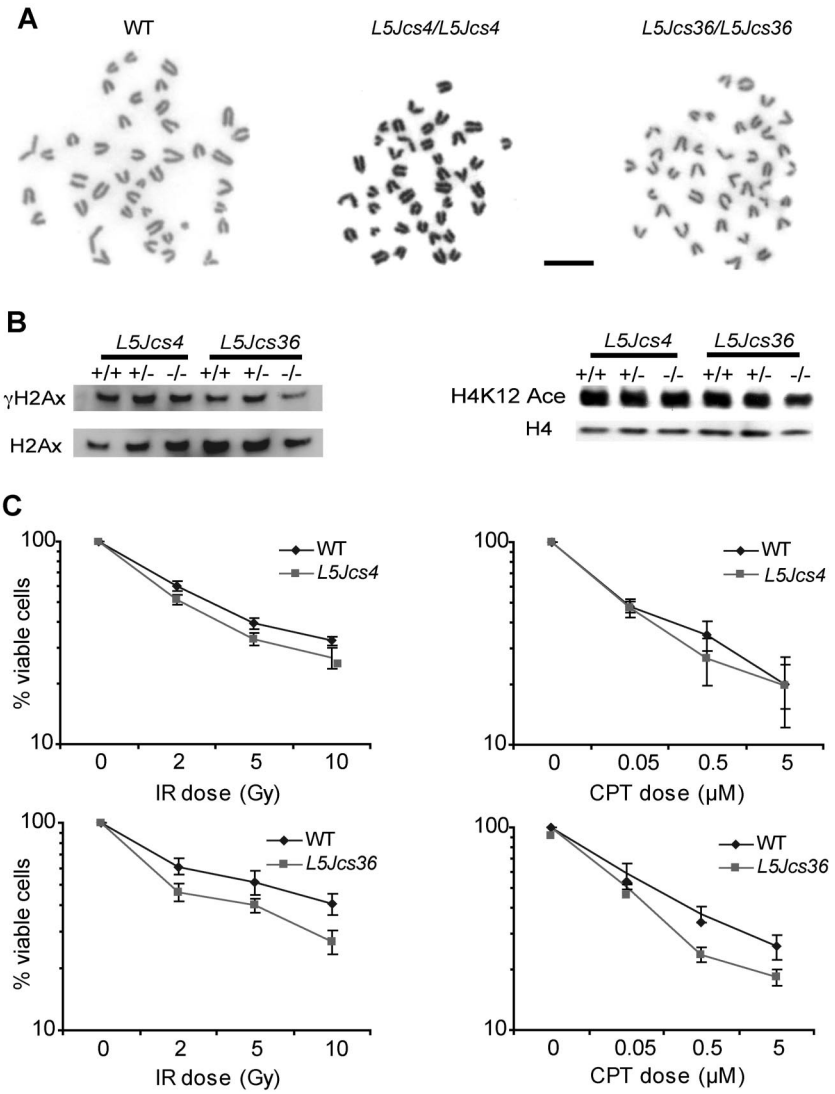

FIG. 10. DNA damage and growth characteristics in *Ptip* mutant cells. (A) Metaphase spreads were prepared from primary cultures of E9.5 embryos and stained with Giemsa. Size bar = 10 μm. (B) Western blot analysis of γH2Ax and H14K12 acetylation. H2Ax and H4 served as loading controls. (C) WT and mutant MEFs were treated with the indicated doses of ionizing radiation (IR) and camptothecin (CPT). Cell viability was assessed 72 h after treatment, and the results are plotted as the percentage of viable cells relative to the results for untreated control cultures. Each point represents the mean ± standard error of the mean of the result. The plots represent three independent MEF cultures for each genotype.

could cause developmental defects ascribed to the combined dysfunction of multiple Pax proteins.

Although BRCT domain-containing proteins are generally associated with DNA damage responses, our studies demonstrate that PTIP has essential functions in development distinct from and in addition to DNA damage repair. The multiple BRCT domain-containing protein TOPBP1 has roles in transcription regulation, DNA replication, and DNA damage checkpoint responses (13). Its three C-terminal BRCT domains directly modulate the activities of several transcription factors (2, 19, 31), including Stromelysin-1 platelet-derived growth factor responsive element binding protein (55), which has no apparent involvement in DNA damage responses. Therefore, it is becoming evident that BRCT domain-containing proteins do not function exclusively in the canonical roles of DNA repair and replication.

The hypomorphic PTIP alleles enabled the uncovering of a wide spectrum of developmental phenotypes, suggesting multiple functions of this protein in regulating embryonic organogenesis and patterning. We have provided evidence that the N- and C-terminal domains are involved in distinct processes. It is intriguing to consider if there is any evolutionary advantage for these functions to reside in the same protein or if there are synergistic functions that are not yet evident.

ACKNOWLEDGMENTS

We thank Gregory Dressler for providing us with *Ptip* knockout mice and anti-mouse PTIP antibody, Xu Peng for helpful discussions, Robert Munroe and Ian Welsh for technical help, and T. O'Brien for advice on the manuscript.

This work was supported by NIH grant R01 HD35984 to J.C.S.

REFERENCES

1. **Adams, R. H., G. A. Wilkinson, C. Weiss, F. Diella, N. W. Gale, U. Deutsch, W. Risau, and R. Klein.** 1999. Roles of ephrinB ligands and EphB receptors in cardiovascular development: demarcation of arterial/venous domains, vascular morphogenesis, and sprouting angiogenesis. Genes Dev. **13:**295–306.
2. **Boner, W., E. R. Taylor, E. Tsirimonaki, K. Yamane, M. S. Campo, and I. M. Morgan.** 2002. A functional interaction between the human papillomavirus 16 transcription/replication factor E2 and the DNA damage response protein TopBP1. J. Biol. Chem. **277:**22297–22303.
3. **Carmeliet, P., V. Ferreira, G. Breier, S. Pollefeyt, L. Kieckens, M. Gertsenstein, M. Fahrig, A. Vandenhoeck, K. Harpal, C. Eberhardt, C. Declercq, J. Pawling, L. Moons, D. Collen, W. Risau, and A. Nagy.** 1996. Abnormal blood vessel development and lethality in embryos lacking a single VEGF allele. Nature **380:**435–439.
4. **Chang, H., D. Huylebroeck, K. Verschueren, Q. Guo, M. M. Matzuk, and A. Zwijsen.** 1999. Smad5 knockout mice die at mid-gestation due to multiple embryonic and extraembryonic defects. Development **126:**1631–1642.
5. **Cho, E. A., M. J. Prindle, and G. R. Dressler.** 2003. BRCT domain-containing protein PTIP is essential for progression through mitosis. Mol. Cell. Biol. **23:**1666–1673.
6. **Conway, S. J., D. J. Henderson, and A. J. Copp.** 1997. Pax3 is required for cardiac neural crest migration in the mouse: evidence from the splotch (Sp2H) mutant. Development **124:**505–514.
7. **Cross, J. C., D. G. Simmons, and E. D. Watson.** 2003. Chorioallantoic morphogenesis and formation of the placental villous tree. Ann. N. Y. Acad. Sci. **995:**84–93.
8. **Dickson, M. C., J. S. Martin, F. M. Cousins, A. B. Kulkarni, S. Karlsson, and R. J. Akhurst.** 1995. Defective haematopoiesis and vasculogenesis in transforming growth factor-beta 1 knock out mice. Development **121:**1845–1854.
9. **Diehl, F., L. Rossig, A. M. Zeiher, S. Dimmeler, and C. Urbich.** 2007. The histone methyltransferase MLL is an upstream regulator of endothelial-cell sprout formation. Blood **109:**1472–1478.
10. **Eklund, L., and B. R. Olsen.** 2006. Tie receptors and their angiopoietin ligands are context-dependent regulators of vascular remodeling. Exp. Cell Res. **312:**630–641.
11. **Ferrara, N., K. Carver-Moore, H. Chen, M. Dowd, L. Lu, K. S. O'Shea, L. Powell-Braxton, K. J. Hillan, and M. W. Moore.** 1996. Heterozygous embryonic lethality induced by targeted inactivation of the VEGF gene. Nature **380:**439–442.
12. **Gale, N. W., M. G. Dominguez, I. Noguera, L. Pan, V. Hughes, D. M. Valenzuela, A. J. Murphy, N. C. Adams, H. C. Lin, J. Holash, G. Thurston, and G. D. Yancopoulos.** 2004. Haploinsufficiency of delta-like 4 ligand results in embryonic lethality due to major defects in arterial and vascular development. Proc. Natl. Acad. Sci. USA **101:**15949–15954.
13. **Garcia, V., K. Furuya, and A. M. Carr.** 2005. Identification and functional analysis of TopBP1 and its homologs. DNA Repair (Amsterdam) **4:**1227–1239.
14. **Glover, J. N., R. S. Williams, and M. S. Lee.** 2004. Interactions between BRCT repeats and phosphoproteins: tangled up in two. Trends Biochem. Sci. **29:**579–585.
15. **Gohler, T., I. M. Munoz, J. Rouse, and J. J. Blow.** 2008. PTIP/Swift is required for efficient PCNA ubiquitination in response to DNA damage. DNA Repair (Amsterdam) **7:**775–787.
16. **Goumans, M. J., F. Lebrin, and G. Valdimarsdottir.** 2003. Controlling the angiogenic switch: a balance between two distinct TGF-b receptor signaling pathways. Trends Cardiovasc. Med. **13:**301–307.
17. **Grailhe, R., C. Waeber, S. C. Dulawa, J. P. Hornung, X. Zhuang, D. Brunner, M. A. Geyer, and R. Hen.** 1999. Increased exploratory activity and altered response to LSD in mice lacking the 5-HT(5A) receptor. Neuron **22:**581–591.
18. **He, C., and X. Chen.** 2005. Transcription regulation of the vegf gene by the BMP/Smad pathway in the angioblast of zebrafish embryos. Biochem. Biophys. Res. Commun. **329:**324–330.
19. **Herold, S., M. Wanzel, V. Beuger, C. Frohme, D. Beul, T. Hillukkala, J. Syvaoja, H. P. Saluz, F. Haenel, and M. Eilers.** 2002. Negative regulation of the mammalian UV response by Myc through association with Miz-1. Mol. Cell **10:**509–521.
20. **Heyer, J., D. Escalante-Alcalde, M. Lia, E. Boettinger, W. Edelmann, C. L. Stewart, and R. Kucherlapati.** 1999. Postgastrulation Smad2-deficient embryos show defects in embryo turning and anterior morphogenesis. Proc. Natl. Acad. Sci. USA **96:**12595–12600.
21. **Hoffmeister, A., A. Ropolo, S. Vasseur, G. V. Mallo, H. Bodeker, B. Ritz-Laser, G. R. Dressler, M. I. Vaccaro, J. C. Dagorn, S. Moreno, and J. L. Iovanna.** 2002. The HMG-I/Y-related protein p8 binds to p300 and Pax2 trans-activation domain-interacting protein to regulate the trans-activation activity of the Pax2A and Pax2B transcription factors on the glucagon gene promoter. J. Biol. Chem. **277:**22314–22319.
22. **Issaeva, I., Y. Zonis, T. Rozovskaia, K. Orlovsky, C. M. Croce, T. Nakamura, A. Mazo, L. Eisenbach, and E. Canaani.** 2007. Knockdown of ALR (MLL2) reveals ALR target genes and leads to alterations in cell adhesion and growth. Mol. Cell. Biol. **27:**1889–1903.
23. **Jeon, S. H., B. C. Chae, H. A. Kim, G. Y. Seo, D. W. Seo, G. T. Chun, N. S. Kim, S. W. Yie, W. H. Byeon, S. H. Eom, K. S. Ha, Y. M. Kim, and P. H. Kim.** 2007. Mechanisms underlying TGF-beta1-induced expression of VEGF and Flk-1 in mouse macrophages and their implications for angiogenesis. J. Leukoc. Biol. **81:**557–566.
24. **Jowsey, P. A., A. J. Doherty, and J. Rouse.** 2004. Human PTIP facilitates ATM-mediated activation of p53 and promotes cellular resistance to ionizing radiation. J. Biol. Chem. **279:**55562–55569.
25. **Krebs, L. T., J. R. Shutter, K. Tanigaki, T. Honjo, K. L. Stark, and T. Gridley.** 2004. Haploinsufficient lethality and formation of arteriovenous malformations in Notch pathway mutants. Genes Dev. **18:**2469–2473.
26. **Krebs, L. T., Y. Xue, C. R. Norton, J. R. Shutter, M. Maguire, J. P. Sundberg, D. Gallahan, V. Closson, J. Kitajewski, R. Callahan, G. H. Smith, K. L. Stark, and T. Gridley.** 2000. Notch signaling is essential for vascular morphogenesis in mice. Genes Dev. **14:**1343–1352.
27. **Lamalice, L., F. Le Boeuf, and J. Huot.** 2007. Endothelial cell migration during angiogenesis. Circ. Res. **100:**782–794.
28. **Larsson, J., M. J. Goumans, L. J. Sjostrand, M. A. van Rooijen, D. Ward, P. Leveen, X. Xu, P. ten Dijke, C. L. Mummery, and S. Karlsson.** 2001. Abnormal angiogenesis but intact hematopoietic potential in TGF-beta type I receptor-deficient mice. EMBO J. **20:**1663–1673.
29. **Lechleider, R. J., J. L. Ryan, L. Garrett, C. Eng, C. Deng, A. Wynshaw-Boris, and A. B. Roberts.** 2001. Targeted mutagenesis of Smad1 reveals an essential role in chorioallantoic fusion. Dev. Biol. **240:**157–167.
30. **Lechner, M. S., I. Levitan, and G. R. Dressler.** 2000. PTIP, a novel BRCT domain-containing protein interacts with Pax2 and is associated with active chromatin. Nucleic Acids Res. **28:**2741–2751.
31. **Liu, K., F. T. Lin, J. M. Ruppert, and W. C. Lin.** 2003. Regulation of E2F1 by BRCT domain-containing protein TopBP1. Mol. Cell. Biol. **23:**3287–3304.
32. **Livak, K. J., and T. D. Schmittgen.** 2001. Analysis of relative gene expression data using real-time quantitative PCR and the 2(-delta delta C(T)) method. Methods **25:**402–408.
33. **Lowndes, N. F., and G. W. Toh.** 2005. DNA repair: the importance of phosphorylating histone H2AX. Curr. Biol. **15:**R99–R102.
34. **Manke, I. A., D. M. Lowery, A. Nguyen, and M. B. Yaffe.** 2003. BRCT repeats as phosphopeptide-binding modules involved in protein targeting. Science **302:**636–639.
35. **Mansouri, A.** 1998. The role of Pax3 and Pax7 in development and cancer. Crit. Rev. Oncog. **9:**141–149.
36. **Massague, J., J. Seoane, and D. Wotton.** 2005. Smad transcription factors. Genes Dev. **19:**2783–2810.
37. **McCarthy, E. E., J. T. Celebi, R. Baer, and T. Ludwig.** 2003. Loss of Bard1, the heterodimeric partner of the Brca1 tumor suppressor, results in early embryonic lethality and chromosomal instability. Mol. Cell. Biol. **23:**5056–5063.
38. **Miller, M.** 2006. Phospho-dependent protein recognition motifs contained in C/EBP family of transcription factors: in silico studies. Cell Cycle **5:**2501–2508.
39. **Miquerol, L., B. L. Langille, and A. Nagy.** 2000. Embryonic development is disrupted by modest increases in vascular endothelial growth factor gene expression. Development **127:**3941–3946.
40. **Mitchell, C. A., C. S. Rutland, M. Walker, M. Nasir, A. J. Foss, C. Stewart, H. Gerhardt, M. A. Konerding, W. Risau, and H. C. Drexler.** 2006. Unique vascular phenotypes following over-expression of individual VEGFA isoforms from the developing lens. Angiogenesis **9:**209–224.
41. **Murr, R., J. I. Loizou, Y. G. Yang, C. Cuenin, H. Li, Z. Q. Wang, and Z. Herceg.** 2006. Histone acetylation by Trrap-Tip60 modulates loading of repair proteins and repair of DNA double-strand breaks. Nat. Cell Biol. **8:**91–99.
42. **Oh, S. P., T. Seki, K. A. Goss, T. Imamura, Y. Yi, P. K. Donahoe, L. Li, K. Miyazono, P. ten Dijke, S. Kim, and E. Li.** 2000. Activin receptor-like kinase 1 modulates transforming growth factor-beta 1 signaling in the regulation of angiogenesis. Proc. Natl. Acad. Sci. USA **97:**2626–2631.
43. **Papaioannou, V. E., and R. R. Behringer.** 2004. Mouse phenotypes: a hand book of mutation analysis. Cold Spring Harbor Laboratory Press, Cold Spring Harbor, NY.
44. **Patel, S. R., D. Kim, I. Levitan, and G. R. Dressler.** 2007. The BRCT-domain containing protein PTIP links PAX2 to a histone H3, lysine 4 methyltransferase complex. Dev. Cell **13:**580–592.
45. **Peters, H., B. Wilm, N. Sakai, K. Imai, R. Maas, and R. Balling.** 1999. Pax1 and Pax9 synergistically regulate vertebral column development. Development **126:**5399–5408.
46. **Ponce, M.** 2000. In vitro matrigel angiogenesis assays, p. 205–209. *In* J. Murray (ed.), Angiogenesis protocols. Humana Press, Totowa, NJ.
47. **Puebla-Osorio, N., D. B. Lacey, F. W. Alt, and C. Zhu.** 2006. Early embryonic lethality due to targeted inactivation of DNA ligase III. Mol. Cell. Biol. **26:**3935–3941.
48. **Rossant, J., and P. P. L. Tam (ed.).** 2002. Mouse development: patterning, morphology, and organogenesis. Academic Press, San Diego, CA.
49. **Sato, T. N.** 1999. Gene trap, gene knockout, gene knock-in, and transgenics in vascular development. Thromb. Haemost. **82:**865–869.

50. **Semenza, G. L.** 1999. Regulation of mammalian O2 homeostasis by hypoxia-inducible factor 1. Annu. Rev. Cell Dev. Biol. **15:**551–578.
51. **Shen, S. X., Z. Weaver, X. Xu, C. Li, M. Weinstein, L. Chen, X. Y. Guan, T. Ried, and C. X. Deng.** 1998. A targeted disruption of the murine Brca1 gene causes gamma-irradiation hypersensitivity and genetic instability. Oncogene **17:**3115–3124.
52. **Shen, T. L., A. Y. Park, A. Alcaraz, X. Peng, I. Jang, P. Koni, R. A. Flavell, H. Gu, and J. L. Guan.** 2005. Conditional knockout of focal adhesion kinase in endothelial cells reveals its role in angiogenesis and vascular development in late embryogenesis. J. Cell Biol. **169:**941–952.
53. **Shi, Y., and J. Massague.** 2003. Mechanisms of TGF-beta signaling from cell membrane to the nucleus. Cell **113:**685–700.
54. **Shimizu, K., P.-Y. Bourillot, S. J. Nielsen, A. M. Zorn, and J. B. Gurdon.** 2001. Swift is a novel BRCT domain coactivator of Smad2 in transforming growth factor β signaling. Mol. Cell. Biol. **21:**3901–3912.
55. **Sjottem, E., C. Rekdal, G. Svineng, S. S. Johnsen, H. Klenow, R. D. Uglehus, and T. Johansen.** 2007. The ePHD protein SPBP interacts with TopBP1 and together they cooperate to stimulate Ets1-mediated transcription. Nucleic Acids Res. **35:**6648–6662.
56. **Spiess, A. N., N. Walther, N. Muller, M. Balvers, C. Hansis, and R. Ivell.** 2003. SPEER–a new family of testis-specific genes from the mouse. Biol. Reprod. **68:**2044–2054.
57. **Stainier, D. Y., B. Fouquet, J. N. Chen, K. S. Warren, B. M. Weinstein, S. E. Meiler, M. A. Mohideen, S. C. Neuhauss, L. Solnica-Krezel, A. F. Schier, F. Zwartkruis, D. L. Stemple, J. Malicki, W. Driever, and M. C. Fishman.** 1996. Mutations affecting the formation and function of the cardiovascular system in the zebrafish embryo. Development **123:**285–292.
58. **Tebbs, R. S., M. L. Flannery, J. J. Meneses, A. Hartmann, J. D. Tucker, L. H. Thompson, J. E. Cleaver, and R. A. Pedersen.** 1999. Requirement for the Xrcc1 DNA base excision repair gene during early mouse development. Dev. Biol. **208:**513–529.
59. **Tremblay, K. D., N. R. Dunn, and E. J. Robertson.** 2001. Mouse embryos lacking Smad1 signals display defects in extra-embryonic tissues and germ cell formation. Development **128:**3609–3621.
60. **Urness, L. D., L. K. Sorensen, and D. Y. Li.** 2000. Arteriovenous malformations in mice lacking activin receptor-like kinase-1. Nat. Genet. **26:**328–331.
61. **Wang, H. U., Z. F. Chen, and D. J. Anderson.** 1998. Molecular distinction and angiogenic interaction between embryonic arteries and veins revealed by ephrin-B2 and its receptor Eph-B4. Cell **93:**741–753.
62. **Weiss, R. S., T. Enoch, and P. Leder.** 2000. Inactivation of mouse Hus1 results in genomic instability and impaired responses to genotoxic stress. Genes Dev. **14:**1886–1898.
63. **Welsh, I. C., and T. P. O'Brien.** 2000. Loss of late primitive streak mesoderm and interruption of left-right morphogenesis in the Ednrb(s-1Acrg) mutant mouse. Dev. Biol. **225:**151–168.
64. **Wilson, L., Y. H. Ching, M. Farias, S. A. Hartford, G. Howell, H. Shao, M. Bucan, and J. C. Schimenti.** 2005. Random mutagenesis of proximal mouse chromosome 5 uncovers predominantly embryonic lethal mutations. Genome Res. **15:**1095–1105.
65. **Wu, Z., H. Guo, N. Chow, J. Sallstrom, R. D. Bell, R. Deane, A. I. Brooks, S. Kanagala, A. Rubio, A. Sagare, D. Liu, F. Li, D. Armstrong, T. Gasiewicz, R. Zidovetzki, X. Song, F. Hofman, and B. V. Zlokovic.** 2005. Role of the MEOX2 homeobox gene in neurovascular dysfunction in Alzheimer disease. Nat. Med. **11:**959–965.
66. **Yang, X., L. H. Castilla, X. Xu, C. Li, J. Gotay, M. Weinstein, P. P. Liu, and C. X. Deng.** 1999. Angiogenesis defects and mesenchymal apoptosis in mice lacking SMAD5. Development **126:**1571–1580.
67. **Yu, Q., Y. Shen, B. Chatterjee, B. H. Siegfried, L. Leatherbury, J. Rosenthal, J. F. Lucas, A. Wessels, C. F. Spurney, Y. J. Wu, M. L. Kirby, K. Svenson, and C. W. Lo.** 2004. ENU induced mutations causing congenital cardiovascular anomalies. Development **131:**6211–6223.
68. **Zlot, C., G. Ingle, J. Hongo, S. Yang, Z. Sheng, R. Schwall, N. Paoni, F. Wang, F. V. Peale, Jr., and M. E. Gerritsen.** 2003. Stanniocalcin 1 is an autocrine modulator of endothelial angiogenic responses to hepatocyte growth factor. J. Biol. Chem. **278:**47654–47659.